ThruMapper: Through-Wall Building Tomography with a Single Mapping Robot

Paper #21: Six pages

Bo Tan
Dept. of Computer Science
University College London
b.tan@cs.ucl.ac.uk

Kevin Chetty
Dept. of Security & Crime Science
University College London
k.chetty@ucl.ac.uk

Kyle Jamieson*
Dept. of Computer Science
University College London
k.jamieson@cs.ucl.ac.uk

ABSTRACT

Vision- and LIDAR-based Simultaneous Localization and Mapping (SLAM) techniques can build indoor building floorplans with ease, but require line-of-sight into every room of a building. We are developing a radio microwave-based system for building indoor floor plans using SLAM techniques, but without the requirement that the mapping robot has access to every room in the building. Our system uses multiple antennas to direct radio energy through walls in particular directions, and joint time- and angle-of-arrival estimation techniques to estimate their backscatter returns from the walls of the building. Wide bandwidth (120 MHz) transmissions combined with an iterative transmit nulling and receive cancellation strategy allows ThruMapper to isolate individual walls and measure the location of a non-line-of-sight wall hidden behind another wall and office clutter to within a 25-centimetre RMS error.

1. Introduction

Indoor navigation is coming of age, with mobile devices now able to guide people to points of interest in shopping centers, airports, and museums. Generally speaking, commercial indoor navigation systems use technology based on overhearing Wi-Fi access points, combined with crowdsourcing information when user density is high, to derive a location fix on a mobile device with 1-2 meters of accuracy, enough for the purpose of finding one's way around a building. A hard requirement of most indoor navigation systems, however, is a map of the building, constructed at a level of accuracy commensurate with navigation precision. Besides presenting the map to the user, indoor navigation systems can leverage a synergistic effect of having a map available, ruling out possible trajectories that pass through walls or other obstacles, and thus improving indoor navigation accuracy.

In new buildings, architectural floorplans are generally easy to obtain in digital form, for import into an indoor navigation product. But in older or historical buildings, or simply when logistics preclude a digital import of floorplans, what can be done? Camera and lidar-based simultaneous localization and mapping (SLAM) is a well-developed family of techniques that leverage cameras or lidar together with robots, to explore and map a space. Loop closure techniques, kinematics modeling, statistical inference, and recursive estimation techniques complement SLAM to achieve impressive results when a robot can visit every room in the space to be mapped. But can a map still be produced when access to every room is more limited, costly, or inconvenient?

Another family of techniques [1] leverages the sensors and radios on users' mobile devices, aggregating people's trajectories as they move through an indoor space, then inferring wall locations based on these crowdsourced movement data. For busy environments where users routinely enter every room, this technique holds promise. But for less busy environments where the amount of data might not be sufficient, or in locations where users' movements do not have a one-to-one correspondence with wall locations, can we produce an accurate map?

This paper presents *ThruMapper*, a microwave radar-based indoor mapping system that addresses the above concerns, producing an indoor map from a wheeled trolley that only needs to be travel through the main corridors of a building, not into every room. Thus doors can stay closed and locked during the system's survey of a building, speeding the process of collecting floorplan data and reducing cost.

ThruMapper works by measuring the backscatter off building walls that arises from its own radio transmissions. Listening radios use phased-array antennas to cancel self-interference from transmitting radios, so that the backscatter signals appear above the very strong self-interference signal. The transmission that ThruMapper uses has a wide 120 MHz bandwidth, so that backscatter readings can provide information about the bearing and range of objects in the environment when coupled with the joint bearing-range estimation algorithms that ThruMapper uses [4]. These techniques alone allow ThruMapper to map out line-of-sight walls in much the same way SLAM algorithms do, but stop short of our main design goal, through-wall mapping. A successive transmit signal nulling and receive signal cancellation strategy allows ThruMapper to leverage joint bearing-range estimation algorithms to see walls behind other walls, eliminating the impact of returns from nearby walls so that the returns from further walls can be discerned. Finally, our mapping algorithms fuse information from the joint bearing-range estimates with small changes in ThruMapper's position measured using inertial and wheel-spin sensors.

We have implemented ThruMapper on a National Instruments USRP-PXI platform containing eight transmit and eight receive radios. Two eight-element Phocus Array 3110X phased-array antennas radiate energy into the office environment where we perform our experimental evaluation. Experimental results demonstrate the ability of ThruMapper's transmitter to effectively null the receiver array as a strategy to suppress the direct signal interference component, which turns out to be critical for ThruMapper to effectively locate both obscuring and obscured walls. Results demonstrate high levels of accuracy: 14 cm RMS error for line-of-sight walls, and 25–57 cm RMS error for walls fully obscured by a line-of-sight wall and other office clutter.

*Also affiliated with the Department of Computer Science, Princeton University (email: kylej@cs.princeton.edu)

2. Design

ThruMapper operates at 2.4 GHz and utilises one 8-element uniform circular phased array (UCA) in transmission, and one in reception. The two UCAs operate in a full-duplex mode and are separated by 70 cm. Moreover, high-bandwidth (120 MHz) waveforms are employed alongside antenna angular nulling techniques and joint space-time estimation algorithms to achieve high range resolutions; minimise interference from the direct signal; and facilitate both angle-of-arrival (AoA) and time-of-fight (ToF) measurements, for estimating bearing and range respectively. ThruMapper is able to identify both the wall closest to itself (termed the *line-of-sight* (*LoS*) wall), and walls located behind the LoS wall, as shown in Figure 1. It can be seen from the figure that ThruMapper uses differing range and bearing measurements to identify the relative locations of maximum reflection from both the LoS wall and second wall (θ_1, τ_1) and (θ_2, τ_2). As the robot moves from its current position P_n to a new location P_{n+1}, the receiving array re-estimates new positions of the walls corresponding to the newly received signals. A full traverse of a wall consisting of P_i measurement positions then permits mapping of the building layout on a two-dimensional grid.

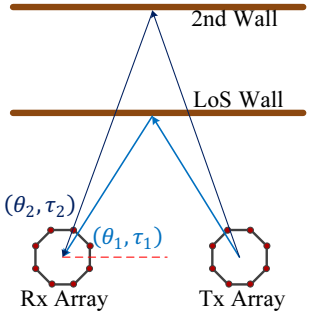

Figure 1— Reflections from a line-of-sight wall and a fully-obscured second wall present different propagation distances and arrival angles to ThruMapper's receiving array.

2.1 Signal Design

As described above, ThruMapper transmits and receives wide-band signals, allowing high accuracy in range estimation, and using eight antennas, allowing high accuracy in angle estimation. Specifically, the transmission signal is divided and sent on different OFDM sub-carriers permitting multiple phase measurements as a function of frequency. Equation 1 describes the signal originating from the transmitting UCA:

$$\boldsymbol{X}(t_0) = \sum_{m=1}^{M} a_m(\theta) \left[1, e^{-j2\pi f_1 t_0}, \ldots, e^{-j2\pi f_N t_0}\right], \quad (1)$$

where $a_m(\theta) = e^{-j\frac{2\pi r}{\lambda} cos\left(\theta - \frac{2\pi m}{M}\right)}$ is the transmitting steering vector with azimuth angle θ, r is the radius of the UCA, λ is the signal wavelength, M is the total number of UCA elements, m is the index of the m^{th} element, and f_i is the frequency of the i^{th} sub-carrier. Accounting for multipath propagation, the signal at the receiving UCA will be the sum of time-delayed versions of $\boldsymbol{X}$ from various angles:

$$\boldsymbol{Y} = [\boldsymbol{a}(\theta_1), \boldsymbol{a}(\theta_2), \ldots \boldsymbol{a}(\theta_L)] \begin{bmatrix} \boldsymbol{X}(t_0 + \tau_1) \\ \boldsymbol{X}(t_0 + \tau_2) \\ \vdots \\ \boldsymbol{X}(t_0 + \tau_L) \end{bmatrix} + \boldsymbol{N} \quad (2)$$

where L is the number of signal paths, N is the noise, and θ_i and τ_i respectively is the AoA and ToF of the signal propagating along the i_{th} path,

$$\boldsymbol{a}(\theta_i) = [a_1(\theta_i), a_2(\theta_i), ..., a_M(\theta_i)]^\top. \quad (3)$$

The effect of a time delay τ_i on one specific sub-carrier f_n is:

$$\varphi_n(\tau_i) = e^{-j2\pi f_n \tau_k} \quad (4)$$

Thus, for a given τ_i, the phase shift linearly increases with the sub-carrier's frequency.

2.2 Joint Space-Time Estimation

To identify and locate both LoS and obscured walls, we employ JADE [4], a subspace technique for joint angle and time delay estimation. JADE is an extension of the well known MUSIC algorithm [3] for estimating the angles of arrival of incoming signals originating from multiple sources, and has been used in [2] for locating 802.11 devices using a space-time smoothing approach. Our design is structured as follows:

Defining the space-time manifold: In a multiple carrier array system, the space-time manifold for a path with AoA θ and ToF τ can be written as:

$$u(\theta, \tau) = a(\theta) \otimes g(\tau) \quad (5)$$

where $\otimes$ is the Kronecker product, $a(\theta)$ is the azimuth angle steering vector defined in (3), and $g(\tau)$ is the time delay manifold defined as $g(\tau) = [1, e^{-j2\pi f_1 \tau}, \ldots, e^{-j2\pi f_N \tau}]$.

Smoothing the received signal: Here we apply a modified version of a linear array smoothing algorithm [2, 5] applicable to circular arrays. Assume $y_{i,j}$ is an entry of the measurement signal $\boldsymbol{Y}$, and subscripts i and j denote antenna index and sub-carrier index respectively. The smoothed measurement matrix can be written as:

$$\boldsymbol{Y_S} = [Y_1, Y_2, ..., Y_M]' \quad (6)$$

where Y_i is the time smoothed measurement matrix for the i_{th} element in array which is defined as:

$$Y_i = \begin{bmatrix} y_{i,1} & y_{i,2} & \cdots & y_{i,N-\frac{N}{p}} \\ y_{i,2} & y_{i,3} & \cdots & y_{i,N-\frac{N}{p}+1} \\ \cdots & & & \cdots \\ y_{i,\frac{N}{p}} & y_{i,\frac{N}{p}+1} & \cdots & y_{i,N} \end{bmatrix} \quad (7)$$

and p is the number of groups for smoothing.

Subspace search: We calculate the auto-correlation matrix $R_{YY} = Y_S Y_S^*$ of the smoothed measurement matrix Y_S (the subsequent eigenvalue decomposition of the R_{YY} and noise subspace E_N are fully described by Schmidt [3]).[1] The range and bearing of the wall reflections from the walls of interest can then be identified by searching for peaks within the space-time surface $P_{\theta,\tau}$:

$$P_{\theta,\tau} = \frac{u^*(\theta,\tau)u(\theta,\tau)}{u^*(\theta,\tau)E_N E_N^* u(\theta,\tau)} \quad (8)$$

2.3 Interference Suppression

Unlike ArrayTrack [5] and Spotfi [2] which work by localising signal sources, the objective of ThruMapper is to detect and localise the much weaker reflections from both the LoS and 2nd walls. A key requirement is therefore to suppress the direct signal interference from the transmitting array into receiving array which can potentially saturate the receiver electronics, and mask the weak echoes

[1] Note that $*$ denotes the conjugate transpose of the matrix.

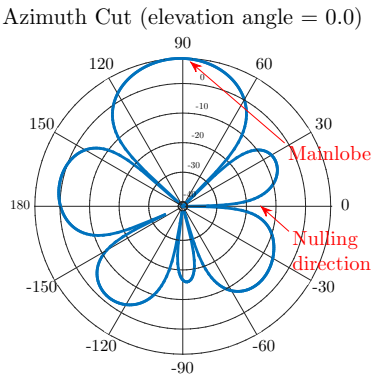

Figure 2— Beam pattern of the transmitting antenna array. An antenna null is steered toward the receiver array at 0°, which is 90° to the mainlobe direction.

from secondary walls beyond the primary wall. Additionally, suppression of the direct signal must be carried out whilst simultaneously cancelling reflections from unwanted scatterers such as those from furniture, stationary objects and people. These objectives are realised using null-steering in the transmitting UCA and interference cancellation in the receiving UCA.

2.3.1 Transmitting Null

The degrees of freedom afforded by array antennas allow their sensitivities to be manipulated as a function of angle. ThruMapper applies the side-lobe cancellation method described in equation 9 to minimise the transmission signal towards the receiving array whilst maximising the antenna gain toward the scene of interest.

$$a_{syn} = a(\theta_d) - a(\theta_n) * \frac{a^*(\theta_n)a(\theta_d)}{a^*(\theta_n)a(\theta_n)} \tag{9}$$

where $a(\theta_d)$ and $a(\theta_n)$ are the steering vectors for the antenna boresight and nulling directions respectively. The simulated antenna beam pattern having a mainlobe at 90° and null at 0° is illustrated in Figure 2. In practice, errors arising from phase drift, thermal noise, and the actual phase calibration procedures typically result in an offset of the measured antenna null angle to that predicted by theory. To counteract this effect, we place RF absorbent material in between the two UCA's.

2.3.2 Received Signal Cancellation

On the receiving UCA, ThruMapper exploits a linear projection method to cancel signals from unwanted range and bearings. After selecting the angles from which undesired responses originate $[\theta_1, \theta_2, ..., \theta_K]$, with corresponding time delays $[\tau_1, \tau_2, ..., \tau_K]$, the following matrix corresponding the the space-time manifold is generated: $\boldsymbol{A} = [u(\theta_1, \tau_1), u(\theta_2, \tau_2), ..., u(\theta_K, \tau_K)]'$. By taking QR decomposition of $\boldsymbol{A}$, we can obtain an orthogonal matrix $\boldsymbol{Q}$. Following the operation in (10)

$$\hat{\boldsymbol{Y}} = \boldsymbol{Q}\boldsymbol{Y} \tag{10}$$

where $\hat{Y}$ is linear projection of $\boldsymbol{Y}$ to the plane orthogonal to $\boldsymbol{A}$. Here, signals arriving from the pre-selected undesired range and bearings have been eliminated. However, in practice we use an iterative approach to remove unwanted scatters.

2.4 Combining Space-Time Information

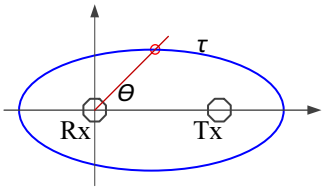

Figure 3— Synthesis of angle-of-arrival and time-of-flight information to determine a reflection point location.

By applying the joint space-time estimation and interference cancellation technique described in Sections 2.2 and 2.3, we obtain the time delay and bearing of the strongest scattering point of the wall, which (ignoring constructive multipath interference) will be equidistant between the transmitting and receiving UCAs (illustrated in Figure 1). The final step in the estimation procedure is to combine the two measurements into a single point within a two-dimensional Cartesian coordinate system: The time delay is converted into an iso-range contour (an ellipsoid with the transmitter and receiver as focal points). Integrating the bearing information as demonstrated by the red line in Figure 3 permits the wall reflection point to be determined.

3. System Implementation

We have built ThruMapper atop a National Instruments (NI) USRP-PXI based wideband multiple radio channel RF system. System control and signal processing functions are implemented in LabVIEW, NI's proprietary software. A block diagram of ThruMapper is shown in Figure 4.

3.1 Hardware

The ThruMapper hardware includes three main sections: (1) Antenna arrays (2) Radio signal generation and acquisition and (3) Signal processing.

Antenna Array: We use two Trimble 8-element Phocus Arrays (3110X), one for transmitting and one for receiving. Each array is designed to operrate within te 2.401 to 2.484 GHz spectral band.

Radio Signal Generation/Acquisition: ThruMapper is built around 8 synchronised NI-USRP (2943R) radio's which act as RF front-ends, and A/D and D/A converters. 4 USRP's make up the transmitting section, and the other 4 make up the receiving section. Each USRP includes two distinct radio channels which can each sample the recieved signal at 120 MS/s IQ.

Signal Processing Unit: The digitized samples from different USRPs are combined via NI-PXIe hub (CPS 8910) then sent to PXI industrial controller (PXIe-8880) for processing. Concurrently, the industrial controller generates pre-DAC samples which are distributed by another PXIe hub to the four transmitting USRPs.

3.2 Software

We use the LabVIEW development environment which provides a graphical user interface, driver and the necessary libraries for device control and signal processing. Before operation, our code runs a various configuration and verification tests to ensure full device control. The algorithms proposed in Section 2 are implemented using LabVIEW's Virtual Instruments, and the subsequent outputs displayed graphically in near real-time.

3.3 Practical Notes

The following notes outline some important strategies that we have undertaken relating to radio synchronisation, calibration and data

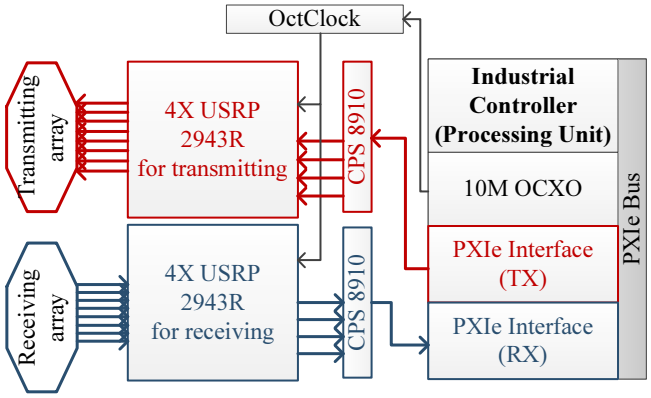

Figure 4— ThruMapper System block diagram

routing for successfully implementing ThruMapper.

Synchronization: The precision of the bearing estimation in Section 2 is dependent on the signal phase measurements in the UCA. Therefore the radio channels associated with each of the eight elements need to be synchronised and phase locked. We use an OctoClock which is driven by a highly stable OCXO 10 MHz clock source to generate eight reference clocks for each USRP. This results in a time-synchronized and phased locked transmitting and receiving array that meets operational requirement specifications.

Calibration: Three additional calibration steps in the set-up phases are necessary and must be implemented in the following order: (i) eliminate the DC offset; (ii) equalise the amplitude bias between channels, and (ii) align signal phases between channels. Though our radio channels are phase locked after synchronization, the initial phase on each radio channel exhibits a random value across power cycles. However this difference is constant during one power cycle. Phase alignment is therefore necessary before signal processing, and this operation must be applied to both UCAs.

Data Routing: The 16 high-bandwidth radio channels used by ThruMapper results in significant data throughput which can overwhelm the PXI bus. To avoid data bottlenecks, time delays have been introduced in the transmit and receive stages prior to the implementation of the first-in-first-out (FIFO) read/write buffer. Moreover, the FIFO size in the USRP's FPGA is modified to work in tandem with the USRPs send and fetch data re-routing functions.

4. Evaluation

This section describes a series of four experiments that have been designed to demonstrate proof-of-concept of ThruMapper. All experiments were carried out within a typical indoor office environment at University College London, and where the radio waves penetrated wall barriers, these were all of 15 cm thickness, and constructed of plasterboard material.

4.1 Nulling the Receive Antenna Array

As described in Section 2.3.1, suppression of the direct signal interference from the transmitting array is vital. The first experiment is therefore designed to verify the ability of the transmitting UCA to null the receiving UCA. The experimental setup is shown in Figure 5a, and the subsequent results in Figure 6. ff

As can be seen from Figure 6, without the application of transmitter nulling towards the receiver, the direct signal interference at 200° appears as a peak in the time-angle JADE surface. After nulling, the signal peak originating from 264° (the direction of the

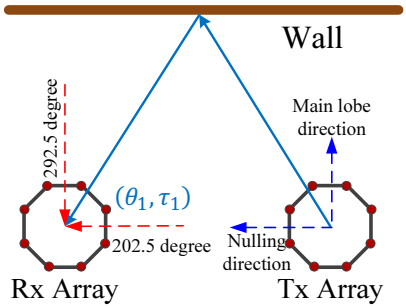

Figure 5— Experimental setup

wall) dominates the JADE output. However we still observe a residual peak at 200° in the second row of Figure 6 (lower). Note that in the JADE surface plot, a unit increase in the ToF index (which corresponding to 2.5 ns) equates to a propagation distance of 75 cm. In the third row of Figure 6 when RF absorber material is used between the UCAs, the direct signal peak is suppressed below the noise floor and can no longer be visualised on the JADE surface. Additionally, the measured ToF difference between the direct and wall-reflection paths is 2.5 ns (75 cm) which is in agreement with the actual path difference of 68 cm. This verifies that joint angle-delay estimation can successfully measure the range of the direct signal and LoS wall reflection.[2]

4.2 Locating the Line-of Sight (LoS) Wall

The second experiment was geared towards identifying the LoS wall at a close and distant range of 70 cm and 220 cm respectively, and the two-way path difference between these geometries was calculated to be 290 cm. Note that for all experiments henceforth, the transmitter array steers a null towards the receiver array. Figure 7a illustrates the ThruMapper system in both the close and distant scenarios. The results in Figure 7 show a reflection path of 268° with a time delay index of seven[3] when the wall is 70 cm away from ThruMapper. This increases to 288° and 11 (angle and time delay index respectively) when ThruMapper is positioned 220 cm away from the wall. After normalising for the 70 cm separation between the two UCA's, the change in the time delay index equates to a two-way path difference of 270 cm, which is in line with expectations, and within the experimental error bounds. The result highlights the high angular- and range-resolution performance of ThruMapper.

4.3 Locating an obscured wall

The third experiment is designed to detect the range and bearing of a secondary wall behind the LoS wall. Our approach involved the application of our received signal cancellation method described in 2.3.2 to iteratively cancel out any unwanted reflections, including that from the LoS wall. Two experimental geometries shown in Figure 8 were examined; the first had a LoS wall to secondary wall separation of 150 cm, whilst the inter-wall separation in the second geometry was 220 cm. ThruMapper was located 70 cm away from the LoS wall in the first geometry, and 80 cm away in the second. From Figure 8b, we observe that the LoS walls appear at expected angles and ToF: 270 degrees and time index 7 for the system at 60 cm stand-off; 275 degrees and time index 7 for the system as 80 cm standoff. The 20 cm position difference between

[2]We note from Figure 6 that the direct transmission between the two arrays (70 cm) causes a delay corresponding to 70 cm of free space propagation, cable propagation and hardware processing time. In the remaining experiments we compensate for this delay in our distance calculations.

[3]In *time delay* units of 2.5 ns.

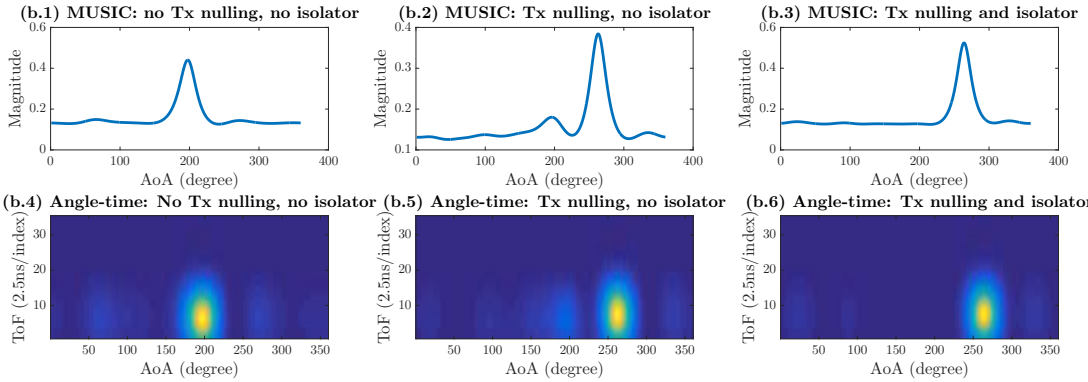

Figure 6— angle detection results (left lower panel) and joint angle-time detection results (right lower panel). **(b.1)** and **(b.4):** No antenna nulling applied to the receiver, **(b.2)** and **(b.5):** application of transmit nulling, **(b.3)** and **(b.6):** Nulling applied with RF absorber.

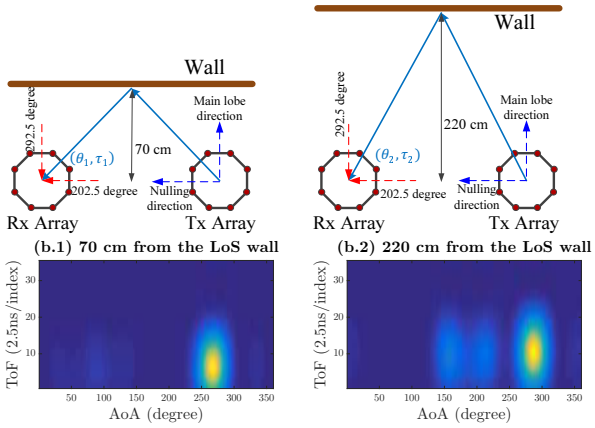

Figure 7— Upper: Experimental setup: 70 cm stand-off (left), 220 cm stand-off (right). **Lower:** Joint angle-time detection results— **(b.1):** 70 cm stand-off (left), **(b.2):** 220 cm stand-off (right)

Wall	Propagation distance	AoA	ToF (by index)
60 cm LoS wall	1.4 m	270	7
80 cm LoS wall	1.75 m	275	7
2.25 m 2nd wall	4.55 m	286	11
3.15 m 2nd wall	6.34 m	277	13

Table 1— AoA and ToF of different walls in Figure 8.

the stand-off positions cannot though be discerned in the results as the 2.5 ns time resolution is equivalent to 75 cm in distance, and thus the LoS wall reflections appear in equivalent range bins. The measured reflected signals from the second wall again exhibit the expected bearing and inter-wall distance within the associated experimental error. 286 degrees and time index 11 for the system at 60 cm stand-off; 277 degrees and time index 13 for the system at an 80 cm standoff. As can be seen from Table 1, ToF estimations closely match with the corresponding location while the AoA estiamtions do not perfectly match with the corresponding location. It is because of during the experiment ThruMapper's two arrays may be not completely parallel with the walls during whole experiment period. This fact will change arrival angle, but not impact ToF.

4.4 Corridor Scanning with ThruMapper

In this experiment ThruMapper moves indoors, taking multiple measurements across a length of wall. The recorded data for both the

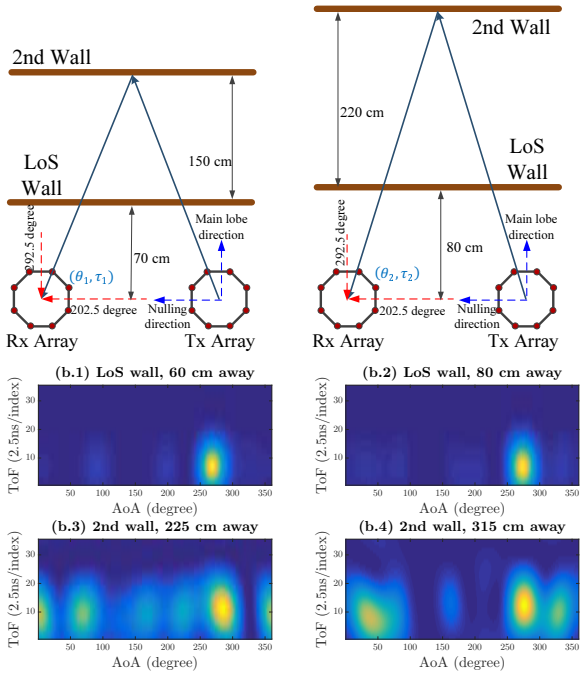

Figure 8— Upper: Experimental setup: 150 cm LoS-2nd wall interval (left), 220 cm LoS-2nd wall interval (right). **Lower:** Joint angle-time estimation of LoS and 2nd wall reflections. **(b.1)** and **(b.2):** AoA and ToF estimation of the LoS walls (60 and 80 cm respectively), **(b.3)** and **(b.4):** AoA and ToF estimation of the second walls (2.25 and 3.15 m respectively).

LoS and secondary wall reflections are then aggregated onto a single 2D grid map using the approach outlined in Section 2.4. This experiment is carried out in an office environment which had an inter-wall distance of 150 cm (Figure 9a).

During the experiment, the mobile platform moved four metres across the room in increments of 20 cm (see Figure 9a), and angle-time data from both the LoS and 2nd walls were collected at each measurement position, denoted by "X" in Figure 9a. The results shown in Figure 9b demonstrate accurate results in the first three metres of the corridor scan. However, between 3-4 meters, there is a marked deviation between the observed and estimated location points for the second wall. We attribute these results to strong returns which ThruMapper encounters as it approaches a corner.

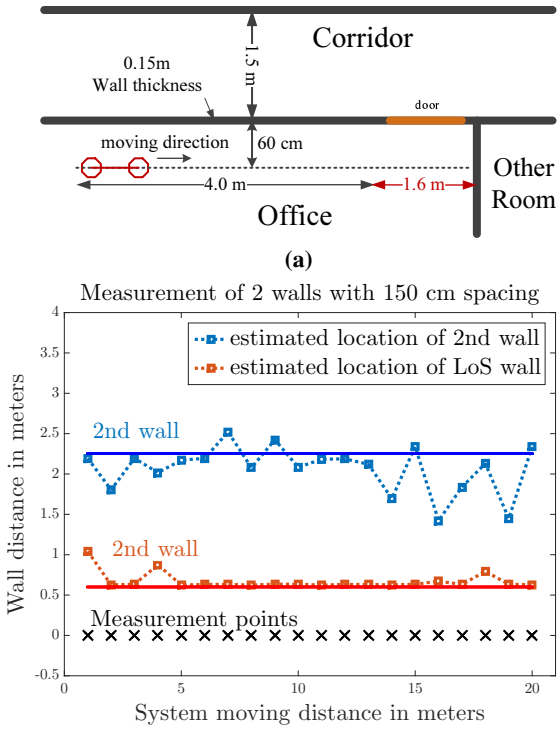

Figure 9— (a) Experimental environment. (b) Location estimation of LoS wall and secondary wall.

4.5 Discussion and Corner Reflections

ThruMapper was put through an experimental measurement campaign to examine its feasibility for through-wall tomography of buildings. Our first experiment (Section 4.1) shows the ability the transmitter to direct an antenna null towards the receiver array in order to suppress the direct signal. The results also highlight the unwanted impact this problematic interference component can have, and thus the need to suppress it. The joint time-angle experiments described in Sections 4.2 and 4.3 then demonstrate that within its range- and angular-resolution capabilities, ThruMapper can detect and locate walls directly in its LoS, as well as obscured secondary walls behind these primary walls, and with an accuracy commensurate to creating useful maps. The last experiment (Section 4.4) showed the ability of ThruMapper to blindly scan a a section of an obscuring primary wall and produce a basic map layout of the room behind it, demonstrating proof-of-concept of the technology. However, it was found that incorrect estimation results were output from ThruMapper as it approached the corner of a wall. Wall corners present a dihedral structure, which are known to have significantly large radar cross sections. We therefore hypothesize that erroneous estimation outputs arise because of the high power returns from corner reflections, which surpass that of the on-axis LoS wall reflections i.e. reflections from the point on the LoS wall that is equidistant from the transmitter and receiver UCA's.

Corner reflection experiments. To examine this phenomenon further, an additional series of measurements were made in the same location (see Figure 9a) to investigate the effect on the LoS wall estimation output when closing-in on the corner reflector. It can be seen in 9a that although the 2nd wall seemed to be affected by the corner of the wall in the 3-4 meter region, reflections from the LoS wall remained dominant throughout the scan. The measurements therefore focused on scanning the LoS wall in the remaining 4 - 5.6m region, again in 20cm increments. Note that results presented in Figure 10 only show the estimated AoA as a function of distance, but do highlight the impact of the corner: Between 4.0m and 4.4m will still observe LoS wall reflections appearing from the expected from the expected 260° region. However, as ThruMapper approaches the corner, dihedral backscatter seems to dominate resulting in returns at shallower angles.

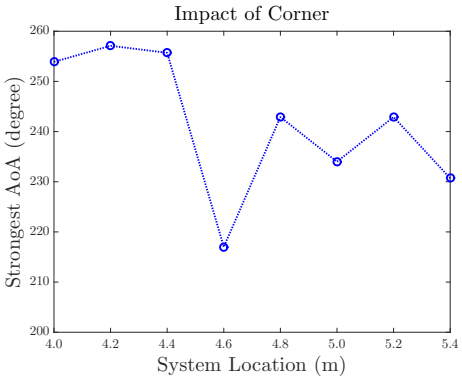

Figure 10— Corner impact on the strongest path AoA

To cope with strong corner reflection, one approach is to identify dihedral structures during a wall/room scan and exploit multiple nulling techniques such as linear constraint minimum variance (LCMV). Another possibility is to leverage the corner return into the SLAM-inspired RF mapping algorithms which we are being developed for ThruMapper. Both strategies are currently being investigated as part of our future work plan.

5. Conclusion

In this work we present ThruMapper; a single robot built around a 16-channel high-bandwidth full-duplex, phased-array radar. We describe the array null steering, interference cancellation, joint angle and time estimation signal processing utilsed by the system, and demonstrate its ability to generate a through-wall tomographic maps of room layout. Our future work will focus on leveraging into our mapping algorithm the high RF backscatter components which arise from the corners of the walls, and build full building floor plans without having to access every room.

Acknowledgments. This research is supported by the National Science Foundation under Grant No. 1617161 and the European Research Council under the EU Seventh Framework Programme (FP/-2007–2013), ERC Grant Agreement No. 279976.

References

[1] M. Alzantot and M. Youssef. Crowdinside: automatic construction of indoor floorplans. In *Proc. of Advances in Geographic Information Systems*, 2012.

[2] M. Kotaru, K. Joshi, D. Bharadia, and S. Katti. Spotfi: Decimeter level localization using wifi. *SIGCOMM Comput. Commun. Rev.*, 45(4):269–282, Aug. 2015.

[3] R. Schmidt. Multiple emitter location and signal parameter estimation. *IEEE Transactions on Antennas and Propagation*, 34(3):276–280, Mar 1986.

[4] A. J. van der Veen, M. C. Vanderveen, and A. Paulraj. Si-jade: an algorithm for joint angle and delay estimation using shift-invariance properties. In *Signal Processing Advances in Wireless Communications, First IEEE Signal Processing Workshop on*, pages 161–164, April 1997.

[5] J. Xiong and K. Jamieson. Arraytrack: A fine-grained indoor location system. In *NSDI*, 2013.